

Response to editor comments

Dear Dr. Kaiser,

Thank you for your valuable input to this manuscript. Your suggestions significantly enhanced the overall quality of our paper. Please see below for a detailed point-by-point response.

1) Please integrate the supplement into the main text as appendix or appendices. The ACP manuscript guidelines require that "Supplementary material is reserved for items that cannot reasonably be included in the main text or as appendices. These may include short videos, very large images, maps, CIF files, as well as short computer codes such as matlab or python script. [...] Normal size figures, tables, as well as technical or theoretical developments that do not need to be included in the main text should be included as appendices."

Thanks for pointing this out. We moved the supplementary material into appendices and main text, now as Appendix A, B and C. We also numbered the figures and equations according to the format guideline.

2) Please remove the unnecessary approximations made in deriving equations 7 and 8, and make them consistent with Eq. 3. I have included the final steps of the calculation without approximation here (using the same δ and ε symbols as in the calculation I sent you during the discussion stage). Obviously, your steps up to the ratio R/R_2 are fine (except that I have used the inverse ratio, to simplify the final step of the calculation): Setting $A = 0$ (very fast isotope exchange) immediately reproduces Eq. 3 for verification.

Thanks for this advice and we agree removing the approximations will making Eq. 2 & 3 consistent with Eq. 7 & 8. In Eq. 7 & 8, we get rid of the approximation that assuming $\delta(\text{NO}_2) - \delta(\text{NO}) = R(\text{NO}_2)/R(\text{NO})$. The non-approximated equation became:

$$\delta(\text{NO}_2) - \delta(\text{NO}) = \frac{(\alpha_2 - \alpha_1) \times A + (\alpha(\text{NO}_2 - \text{NO}) - 1)}{\alpha_1 A + 1} (1 + \delta(\text{NO}))$$

Here, when $A=0$, Eq. 7 become Eq. 2, therefore the two sets of equations are consistent.

However, we suggest the approximation that $\alpha_1 * A + 1 = A + 1$ can still be applied since it introduces very little error and will greatly simplify the equation by reducing the number of unknowns. We calculated the $\delta(\text{NO}_2) - \delta(\text{NO})$ values before and after this approximation by assuming $\alpha_1 = 1.005$, which is an overestimation because our theoretical calculations show that it should only range from 1.0025 to 1.0029. Even under this assumption, we can calculate that the differences between approximation vs. non-approximation was less than 0.05‰ (with A ranging from 0.001 to 500). This difference is much smaller than the analytical uncertainty in many labs so it can be neglected. In the meantime, if we use this assumption ($\alpha_1 * A = A$), we can mathematically reduce the number of unknowns from two ($\alpha_2 - \alpha_1$ and α_1) to one (treating $\alpha_2 - \alpha_1$ as one number). This approximation emphasized that the $\alpha_2 - \alpha_1$ value, or the LCIE factor, acted as one important factor. Therefore, we suggest applying this approximation can simplify our model without bringing much uncertainty.

3) There is no need to repeat the reaction equations (R1 to R6, p. 5 of current supplement) or the definition of delta values (p. 6 of current supplement, lines from "Next, to calculate ..." to " $R_{\text{NO}_2}/R_{\text{NO}} - 1$ ") in the Appendix.

In the appendix, we removed R1-R6 and referred the reactions to the main text. We also removed the delta definition equations.

4) Please remove unnecessary factors ("1000 ‰") from your mathematical equations (e.g. l. 180 and 182).

Revised as suggested.

5) Please also remove the unnecessary multiplication symbols (\times). These make the equations unnecessarily difficult to read. Such multiplication symbols are rarely required outside scientific notation, e.g. $8 \times 10^{-14} \text{ cm}^3 \text{ s}^{-1}$.

Revised as suggested.

6) L. 182: The quantity with the symbol ε should not be called "isotope enrichment factor" (which is a different kind of quantity). Please use the term "equilibrium isotopic fractionation" instead (as you do on l. 89 and elsewhere).

Thanks for pointing this out. In the text, we replaced all ε symbols with $\alpha-1$ since we do not really need this extra symbol. Then, we name α "equilibrium fractionation factor"

7) L. 188 & 193: The quantities should be enclosed in parentheses so that the unit applies to value and uncertainty, e.g. " $(-58.7 \pm 0.8) \text{ ‰}$ "

Revised as suggested.

List of changes

1. The supplementary material now is merged into the main text or as appendices.
2. A more precise equation 7 is used in the main text.
3. Improvement was made in mathematical expressions, such as removing “1000%”, “×”, and including uncertainties in brackets.
4. Replaced symbol “ ε ” with “ α ” to represent the equilibrium fractionation factor.
5. Reference list was updated to match the formatting requirement.

1 **Quantifying the nitrogen isotope effects during photochemical**
2 **equilibrium between NO and NO₂: implications for δ¹⁵N in**
3 **tropospheric reactive nitrogen**

4 Jianghanyang Li¹, Xuan Zhang², John Orlando², Geoffrey Tyndall² and Greg Michalski^{1,3}

5 ¹. Department of Earth, Atmospheric and Planetary Sciences, Purdue University, West Lafayette,
6 IN, 47907

7 ². Atmospheric Chemistry Observations and Modeling Lab, National Center for Atmospheric
8 Research, Boulder, CO, 80301

9 ³. Department of Chemistry, Purdue University, West Lafayette, IN, 47907

10 *Correspondence to:* Jianghanyang Li (li2502@purdue.edu)

11 **Abstract.** Nitrogen isotope fractionations between nitrogen oxides (NO and NO₂) play a
12 significant role in determining the nitrogen isotopic compositions (δ¹⁵N) of atmospheric reactive
13 nitrogen. Both the equilibrium isotopic exchange between NO and NO₂ molecules and the isotope
14 effects occurring during the NO_x photochemical cycle are important, but both are not well
15 constrained. The nighttime and daytime isotopic fractionations between NO and NO₂ in an
16 atmospheric simulation chamber at atmospherically relevant NO_x levels were measured. Then, the
17 impact of NO_x level and NO₂ photolysis rate to the combined isotopic fractionation (equilibrium
18 isotopic exchange and photochemical cycle) between NO and NO₂ were calculated. It was found
19 that the isotope effects occurring during the NO_x photochemical cycle can be described using a
20 single fractionation factor, designated the Leighton Cycle Isotope Effect (LCIE). The results
21 showed that at room temperature, the fractionation factor of nitrogen isotopic exchange is
22 1.0275±0.0012, and the fractionation factor of LCIE (when O₃ solely controls the oxidation from
23 NO to NO₂) is 0.990±0.005. The measured LCIE factor showed good agreement with previous
24 field measurements, suggesting that it could be applied in ambient environment, although future
25 work is needed to assess the isotopic fractionation factors of NO + RO₂/HO₂ → NO₂. The results
26 were used to model the NO-NO₂ isotopic fractionations under several NO_x conditions. The model
27 suggested that isotopic exchange was the dominate factor when NO_x >20 nmol mol⁻¹, while LCIE
28 was more important at low NO_x concentrations (<1 nmol mol⁻¹) and high rates of NO₂ photolysis.
29 These findings provided a useful tool to quantify the isotopic fractionations between tropospheric
30 NO and NO₂, which can be applied in future field observations and atmospheric chemistry models.
31

32

33 1. Introduction

34 The nitrogen isotopic composition ($\delta^{15}\text{N}$) of reactive nitrogen compounds in the
35 atmosphere is an important tool in understanding the sources and chemistry of atmospheric NO_x
36 ($\text{NO}+\text{NO}_2$). It has been suggested that the $\delta^{15}\text{N}$ value of atmospheric nitrate (HNO_3 , nitrate
37 aerosols and nitrate ions in the precipitation and snow) imprints the $\delta^{15}\text{N}$ value of NO_x sources
38 (Elliott et al., 2009; Kendall et al., 2007) thus many studies have used the $\delta^{15}\text{N}$ values of
39 atmospheric nitrate to investigate NO_x sources (Chang et al., 2018; Felix et al., 2012; Felix &
40 Elliott, 2014; Gobel et al., 2013; Hastings et al., 2004, 2009; Morin et al., 2009; Park et al., 2018;
41 Walters et al., 2015, 2018). However, there remain questions about how isotopic fractionations
42 that may occur during photochemical cycling of NO_x could alter the $\delta^{15}\text{N}$ values as it partitions
43 into NO_y (NO_y = atmospheric nitrate, NO_3 , N_2O_5 , HONO , etc., Chang et al., 2018; Freyer, 1991;
44 Hastings et al., 2004; Jarvis et al., 2008; Michalski et al., 2005; Morin et al., 2009; Zong et al.,
45 2017). Similarly, other complex reactive nitrogen chemistry, such as nitrate photolysis and re-
46 deposition in ice and snow (Frey et al., 2009), may impact the $\delta^{15}\text{N}$ of NO_y and atmospheric nitrate.
47 The fractionation between NO and NO_2 via isotope exchange has been suggested to be the
48 dominant factor in determining the $\delta^{15}\text{N}$ of NO_2 and ultimately atmospheric nitrate (Freyer, 1991;
49 Freyer et al., 1993; Savarino et al., 2013; Walters et al., 2016). However, isotopic fractionations
50 occur in most, if not all, NO_x and NO_y reactions, while most of these are still unknown or, if
51 calculated (Walters and Michalski, 2015), unverified by experiments. Since the atmospheric
52 chemistry of NO_y varies significantly in different environments (e.g., polluted vs. pristine, night
53 vs. day), the isotopic fractionations associated with NO_y chemistry are also likely to vary in
54 different environments. These unknowns could potentially bias conclusions about NO_x source
55 apportionment reached when using nitrogen isotopes. Therefore, understanding the isotopic

56 fractionations between NO and NO₂ during photochemical cycling could improve our
57 understanding of the relative role of sources versus chemistry for controlling the δ¹⁵N variations
58 of atmospheric NO₂ and nitrate.

59 In general, there are three types of isotopic fractionation effects associated with NO_x
60 chemistry (Fig. 1A). The first type is the equilibrium isotopic effect (EIE), i.e., isotope exchange
61 between two compounds without forming new molecules (Urey, 1947, Bigeleisen and Mayer,
62 1947), which for nitrogen isotopes in the NO_x system is the $^{15}\text{NO} + ^{14}\text{NO}_2 \leftrightarrow ^{14}\text{NO} + ^{15}\text{NO}_2$
63 exchange reaction (Begun and Melton, 1956, Walters et al., 2016). The second type is the kinetic
64 isotopic effect (KIE) associated with difference in isotopologue rate coefficients during
65 unidirectional reactions (Bigeleisen & Wolfsberg, 1957). In the NO_x system this KIE would
66 manifest in the oxidation of NO into NO₂ by O₃/HO₂/RO₂. The third type is the photochemical
67 isotope fractionation effect (PHIFE, Miller & Yung, 2000), which for NO_x is the isotopic
68 fractionation associated with NO₂ photolysis. All three fractionations could impact the δ¹⁵N value
69 of NO₂, and consequently atmospheric nitrate, but the relative importance of each may vary.

70 The limited number of studies on the EIE in the NO_x cycle have significant uncertainties.
71 Discrepancies in the EIE for $^{15}\text{NO} + ^{14}\text{NO}_2 \leftrightarrow ^{14}\text{NO} + ^{15}\text{NO}_2$ have been noted in several studies.
72 Theoretical calculations predicted isotope fractionation factors (α) ranging from 1.035 to 1.042 at
73 room temperature (Begun & Fletcher, 1960; Monse et al., 1969; Walters & Michalski, 2015) due
74 to the different approximations used to calculate harmonic frequencies in each study. Likewise,
75 two separate experiments measured different room temperature fractionation factors of
76 1.028 ± 0.002 (Begun & Melton, 1956) and 1.0356 ± 0.0015 (Walters et al., 2016). A concern in both
77 experiments is that they were conducted in small chambers with high NO_x concentrations
78 (hundreds of μmol mol⁻¹), significantly higher than typical ambient atmospheric NO_x levels

79 (usually less than $0.1 \mu\text{mol mol}^{-1}$). Whether the isotopic fractionation factors determined by these
80 experiments are applicable in the ambient environment is uncertain because of possible wall effects
81 and formation of higher oxides, notably N_2O_4 and N_2O_3 at these high NO_x concentrations.

82 Even less research has examined the KIE and PHIFE occurring during NO_x cycling. The
83 KIE of $\text{NO} + \text{O}_3$ has been theoretically calculated (Walters and Michalski, 2016) but has not been
84 experimentally verified. The NO_2 PHIFE has not been experimentally determined or theoretically
85 calculated. As a result, field observation studies often overlook the effects of PHIFE and KIE.
86 Freyer et al. (1993) measured NO_x concentrations and the $\delta^{15}\text{N}$ values of NO_2 over a 1-year period
87 at Jülich, Germany and inferred a combined NO_x isotope fractionation factor (EIE+KIE+PHIFE)
88 of 1.018 ± 0.001 . Freyer et al. (1993) suggested that the NO_x photochemical cycle (KIE and PHIFE)
89 tends to diminish the equilibrium isotopic fractionation (EIE) between NO and NO_2 . Even if this
90 approach were valid, applying this single fractionation factor elsewhere, where NO_x , O_3
91 concentrations and actinic fluxes are different, would be tenuous given that these factors may
92 influence the relative importance of EIE, KIE and PHIFE (Hastings et al., 2004; Walters et al.,
93 2016). Therefore, to quantify the overall isotopic fractionations between NO and NO_2 at various
94 tropospheric conditions, it is crucial to know 1) isotopic fractionation factors of EIE, KIE and
95 PHIFE individually and 2) the relative importance of each factor under various conditions.

96 In this work, we aim to quantify the nitrogen isotope fractionation factors between NO and
97 NO_2 at photochemical equilibrium. First, we measure the N isotope fractionations between NO
98 and NO_2 in an atmospheric simulation chamber at atmospherically relevant NO_x levels. Then, we
99 provide mathematical solutions to assess the impact of NO_x level and NO_2 photolysis rate ($j(\text{NO}_2)$)
100 to the relative importance of EIE, KIE and PHIFE. Subsequently we use the solutions and chamber
101 measurements to calculate the isotopic fractionation factors of EIE, KIE and PHIFE. Lastly, using

102 the calculated fractionation factors and the equations, we model the NO-NO₂ isotopic
103 fractionations at several sites to illustrate the behavior of δ¹⁵N values of NO_x in the ambient
104 environment.

105

106 2. Methods

107 The experiments were conducted using a 10 m³ Atmospheric Simulation Chamber at the
108 National Center for Atmospheric Research (see descriptions in [Appendix A](#) and Zhang et al.
109 (2018)). A set of mass flow controllers was used to inject NO and O₃ into the chamber. NO was
110 injected at 1 L min⁻¹ from an in-house NO/N₂ cylinder (133.16 μmol mol⁻¹ NO in ultra-pure N₂),
111 and O₃ was generated by flowing 5 L min⁻¹ zero-air through a flow tube equipped with a UV Pen-
112 Ray lamp (UVP LLC., CA) into the chamber. NO and NO₂ concentrations were monitored in real
113 time by chemiluminescence with a detection limit of 0.5 ppb (model CLD 88Y, Eco Physics, MI)
114 as were O₃ concentrations using an UV absorption spectroscopy with a detection limit of 0.5 ppb
115 (model 49, Thermo Scientific, CO). In each experiment, the actual amounts of NO and O₃ injected
116 were calculated using measured NO_x and O₃ concentrations after steady state was reached (usually
117 within 1 h). The wall loss rate of NO₂ was tested by monitoring O₃ (29 nmol mol⁻¹) and NO_x (62
118 nmol mol⁻¹) over a 4-hour period. After the NO and NO₂ concentrations reached steady state, no
119 decrease in NO₂ concentrations was observed showing that chamber wall loss was negligible.

120 Two sets of experiments were conducted to separately investigate the EIE, KIE and PHIFE.
121 The first set of experiments was conducted in the dark. In each of these dark experiments, a range
122 of NO and O₃ ([O₃] < [NO]) was injected into the chamber to produce NO-NO₂ mixtures with
123 [NO]/[NO₂] ratios ranging from 0.43 to 1.17. The N isotopes of these mixtures were used to
124 investigate the EIE between NO and NO₂. The second set of experiments was conducted under

Deleted: supplementary material

126 irradiation of UV lights (300-500 nm, see [Appendix A](#) for irradiation spectrum). Under such
127 conditions, NO, NO₂ and O₃ reached photochemical steady state, which combined the isotopic
128 effects of EIE, KIE and PHIFE. In addition, three experiments were conducted to measure the δ¹⁵N
129 value of the tank NO. In each of these experiments, a certain amount of O₃ was first injected into
130 the chamber, then approximately the same amount of NO was injected into the chamber to ensure
131 100% of the NO_x was in the form of NO₂ with little O₃ (<3 nmol mol⁻¹) remaining in the chamber,
132 such that the O₃+NO₂ reaction was negligible. The NO₂ in the chamber was then collected and its
133 δ¹⁵N value measured, which equates to the δ¹⁵N value of the tank NO.

Deleted: supplementary material

134 In all experiments, the concentrations of NO, NO₂ and O₃ were allowed to reach steady
135 state, and the product NO₂ was collected from the chamber using a honeycomb denuder tube. [After](#)
136 [the NO, NO₂ and O₃ concentrations reached steady-state, well-mixed chamber air was drawn out](#)
137 [through a Norprene Thermoplastic tubing ~40 cm at 10 L min⁻¹ and passed through a honeycomb](#)
138 [denuder system \(Chemcomb 3500, Thermo Scientific\). Based on flow rate, the NO₂ residence time](#)
139 [in the was less than 0.5 second, thus in the light-on experiments where NO and O₃ coexisted, the](#)
140 [NO₂ produced inside the transfer tube through NO+O₃ reactions should be <0.03 ppb \(using the](#)
141 [upper limit of NO and O₃ concentrations in our experiments\). The honeycomb denuder system](#)
142 [consisted of two honeycomb denuder tubes connected in series. Each honeycomb denuder tube is](#)
143 [a glass cylinder of 38 mm long, 47 mm in diameter, and consist of 212 hexagonal tubes with inner](#)
144 [diameters of 2 mm. Before collecting samples, each denuder tube was coated with a solution of](#)
145 10% KOH and 25% guaiacol in methanol and then dried by flowing N₂ gas through the denuder
146 tube for 15 seconds (Williams and Grosjean, 1990, Walters et al., 2016). The NO₂ reacted with
147 guaiacol coating and was converted into NO₂⁻ that was retained on the denuder tube wall (Williams
148 and Grosjean, 1990). NO was inert to the denuder tube coating: a control experiment sampled pure

Deleted: The glass denuder tubes

Deleted: (Chemcomb 3500, Thermo Fisher Scientific) were ...

153 NO using the denuder tubes, which did not show any measurable NO_2^- . The NO_2 collection
154 efficiency of a single honeycomb denuder tube was tested in another control experiment: air
155 containing 66 nmol mol^{-1} of NO_2 was drawn out of the chamber through a denuder tube, and the
156 NO_2 concentration at the exit of the tube holder was measured and found to be below the detection
157 limit ($<1 \text{ nmol mol}^{-1}$), suggesting the collection efficiency was nearly 100% when $[\text{NO}_2] < 66 \text{ nmol}$
158 mol^{-1} . Furthermore, when the denuder system consisted of two denuder tubes in series and NO_2^- in
159 the second denuder was below the detection limit indicating trivial NO_2 breakthrough. Each NO_2
160 collection lasted for 0.5-3 hours in order to collect enough NO_2^- for isotopic analysis (~300 nmol).
161 After collection, the NO_2^- was leached from each denuder tube by rinsing thoroughly with 10 ml
162 deionized water into a clean polypropylene container and stored frozen until isotopic analysis.
163 Isotopic analysis was conducted at Purdue Stable Isotope Laboratory. For each sample,
164 approximately 50 nmol of the NO_2^- extract was mixed with 2 M sodium azide solution in acetic
165 acid buffer in an air-tight glass vial, then shaken overnight to completely reduce all the NO_2^- to
166 $\text{N}_2\text{O}_{(g)}$ (Casciotti & McIlvin, 2007; McIlvin & Altabet, 2005). The product N_2O was directed into
167 a Thermo GasBench equipped with cryo-trap, then the $\delta^{15}\text{N}$ of the N_2O was measured using a
168 Delta-V Isotope Ratios Mass Spectrometer. Six coated denuders tubes that did not get exposed to
169 NO_2 were also analyzed using the same chemical procedure, which did not show any measurable
170 signal on the IRMS, suggesting the blank from both sampling process and the chemical conversion
171 process was negligible. The overall analytical uncertainty for $\delta^{15}\text{N}$ analysis was 0.5 ‰ (1 σ) based
172 on replicate analysis of in house NO_2^- standards.

Deleted: The

Deleted: ±

173

174 3. Results and Discussions

175 3.1. Equilibrium Isotopic Fractionation between NO and NO_2

178 The equilibrium isotope fractionation factor, $\alpha(\text{NO}_2\text{-NO})$, is the ^{15}N enrichment in NO_2
 179 relative to NO , and is expressed as the ratio of rate constants k_2/k_1 of two reactions:



182 where k_1 is the rate constant of the isotopic exchange, which was previously determined to be
 183 $8.14 \times 10^{-14} \text{ cm}^3 \text{ s}^{-1}$ (Sharma et al., 1970). The reaction time required for NO-NO_2 to reach isotopic
 184 equilibrium was estimated using the exchange rate constants in a simple kinetics box model
 185 (BOXMOX, Knote et al., 2015). The model predicts that at typical NO_x concentrations used during
 186 the chamber experiments ($7.7\text{-}62.4 \text{ nmol mol}^{-1}$), isotopic equilibrium would be reached within 15
 187 minutes (see [Appendix B](#)). Since the sample collection usually started 1 hour after NO_x was well
 188 mixed in the chamber, there was sufficient time to reach full isotope equilibrium. The isotope
 189 equilibrium fractionation factor ($\alpha(\text{NO}_2\text{-NO})$) is then calculated to be:

190
$$\alpha(\text{NO}_2 - \text{NO}) = \frac{[^{15}\text{NO}_2][^{14}\text{NO}]}{[^{14}\text{NO}_2][^{15}\text{NO}]} = \frac{R(\text{NO}_2)}{R(\text{NO})}$$
 Eq. (1)

191 where $R(\text{NO}, \text{NO}_2)$ are the $^{15}\text{N}/^{14}\text{N}$ ratios of NO and NO_2 . By definition, the
 192 $\delta^{15}\text{N}(\text{NO}) = (R(\text{NO})/R(\text{reference}) - 1) \times 1000 \text{ ‰}$ and $\delta^{15}\text{N}(\text{NO}_2) = (R(\text{NO}_2)/R(\text{reference}) - 1) \times 1000 \text{ ‰}$,
 193 but hereafter, the $\delta^{15}\text{N}$ values of NO , NO_2 and NO_x will be referred as $\delta(\text{NO})$, $\delta(\text{NO}_2)$ and $\delta(\text{NO}_x)$,
 194 respectively. Eq. (1) leads to:

195
$$\delta(\text{NO}_2) - \delta(\text{NO}) = (\alpha(\text{NO}_2 - \text{NO}) - 1) \times (1 + \delta(\text{NO}))$$
 Eq. (2)

196 Using Eq. (2) and applying NO_x isotopic mass balance ($\delta(\text{NO}_x) = f(\text{NO}_2)\delta(\text{NO}_2) + (1 - f(\text{NO}_2))\delta(\text{NO})$),
 197 $f(\text{NO}_2) = [\text{NO}_2]/([\text{NO}] + [\text{NO}_2])$ yields:

198
$$\frac{\delta(\text{NO}_2) - \delta(\text{NO}_x)}{1 + \delta(\text{NO}_2)} = \frac{\alpha(\text{NO}_2 - \text{NO}) - 1}{\alpha(\text{NO}_2 - \text{NO})} (1 - f(\text{NO}_2))$$
 Eq. (3)

Deleted: ×

Deleted: supplementary materi

Deleted: al

Formatted: Indent: Left: 0.5"

Deleted: ×

Deleted: ×

Deleted: × 1000 ‰ ×

Deleted: $\epsilon(\text{NO}_2 - \text{NO}) = (\alpha(\text{NO}_2 - \text{NO}) - 1) \times 1000 \text{ ‰}$

Formatted: Indent: Left: 0.5"

Deleted: where $\epsilon(\text{NO}_2\text{-NO})$ is the isotope enrichment factor ($\epsilon(\text{NO}_2\text{-NO}) = (\alpha(\text{NO}_2\text{-NO}) - 1) \times 1000 \text{ ‰}$, Hoefs, 2009).

Deleted: ×

Deleted: ×

Formatted: Indent: Left: 1", First line: 0.5"

211 Here, $\delta(\text{NO}_x)$ equals to the $\delta^{15}\text{N}$ value of the cylinder NO and $f(\text{NO}_2)$ is the molar fraction of NO_2
212 with respect to total NO_x . Three experiments (see descriptions in method section) that measured
213 $\delta(\text{NO}_x)$ showed consistent $\delta(\text{NO}_x)$ values of $(-58.7 \pm 0.8) \text{‰}$ ($n = 3$), indicating $\delta(\text{NO}_x)$ remained
214 unchanged throughout the experiments (as expected for isotope mass balance). Thus, the $\delta(\text{NO}_x)$
215 can be treated as a constant in Eq. (3), and the linear regression of $(\delta(\text{NO}_2) - \delta(\text{NO}_x)) / (1 + \delta(\text{NO}_2))$
216 versus $1 - f(\text{NO}_2)$ should have an intercept of 0 and a slope of $(\alpha(\text{NO}_2 - \text{NO}) - 1) / \alpha(\text{NO}_2 - \text{NO})$.

Deleted: $\varepsilon(\text{NO}_2 - \text{NO}) / (1 + \varepsilon(\text{NO}_2 - \text{NO}))$

217 The plot of $(\delta(\text{NO}_2) - \delta(\text{NO}_x)) / (1 + \delta(\text{NO}_2))$ as a function of $1 - f(\text{NO}_2)$ values from five
218 experiments yields an $\alpha(\text{NO}_2 - \text{NO})$ value of 1.0275 ± 0.0012 at room temperature (Fig. 1B). This
219 fractionation factor is comparable to previously measured values but with some differences. Our
220 result agrees well with the $\alpha(\text{NO}_2 - \text{NO})$ value of 1.028 ± 0.002 obtained by Begun and Melton (1956)
221 at room temperature. However, Walters et al., (2016) determined the $\alpha(\text{NO}_2 - \text{NO})$ values of NO -
222 NO_2 exchange in a 1-liter reaction vessel, which showed a slightly higher $\alpha(\text{NO}_2 - \text{NO})$ value of
223 1.035. This discrepancy might originate from rapid heterogeneous reactions on the wall of the
224 reaction vessel at high NO_x concentrations and the small chamber size used by Walters et al. (2016).
225 They used a reaction vessel made of Pyrex, which is known to absorb water (Do Remus et al.,
226 1983; Takei et al., 1997) that can react with NO_2 forming HONO, HNO_3 and other N compounds.
227 Additionally, previous studies have suggested that Pyrex walls enhance the formation rate of N_2O_4
228 by over an order of magnitude (Barney & Finlayson-Pitts, 2000; Saliba et al., 2001), which at
229 isotopic equilibrium is enriched in ^{15}N compared to NO and NO_2 (Walters & Michalski, 2015).
230 Therefore, their measured $\alpha(\text{NO}_2 - \text{NO})$ might be slightly higher than the actual $\alpha(\text{NO}_2 - \text{NO})$ value.
231 In this work, the 10 m^3 chamber has a much smaller surface to volume ratio relative to Walters et
232 al. (2016) which minimizes wall effects, and the walls were made of Teflon that minimize NO_2
233 surface reactivity, which was evidenced by the NO_2 wall loss control experiment. Furthermore,

Deleted: ε

Deleted: $27.5 \pm 1.2 \text{‰}$

237 the low NO_x mixing ratios in our experiments minimized N₂O₄ and N₂O₃ formation. At NO and
238 NO₂ concentrations of 50 nmol mol⁻¹ the steady state concentrations of N₂O₄ and N₂O₃ were
239 calculated to be 0.014 and 0.001 pmol mol⁻¹, respectively (Atkinson et al., 2004). Therefore, we
240 suggest our measured $\alpha(\text{NO}_2\text{-NO})$ value (1.0275±0.0012) may better reflect the room temperature
241 (298 K) NO-NO₂ EIE in the ambient environment.

242 Unfortunately, the chamber temperature could not be controlled so we were not able to
243 investigate the temperature dependence of the EIE. Hence, we speculate that the $\alpha(\text{NO}_2\text{-NO})$
244 follows a similar temperature dependence pattern calculated in Walters et al. (2016). Walters et al.
245 (2016) suggested that, the $\alpha(\text{NO}_2\text{-NO})$ value would be 0.0047 higher at 273 K and 0.002 lower at
246 310 K, relative to room temperature (298 K). Using this pattern and our experimentally determined
247 data, we suggest the $\alpha(\text{NO}_2\text{-NO})$ values at 273 K, 298 K and 310 K are 1.0322±0.0012,
248 1.0275±0.0012, and 1.0255±0.0012, respectively. This 0.0067 variation at least partially contribute
249 to the daily and seasonal variations of $\delta^{15}\text{N}$ values of NO₂ and nitrate in some areas (e.g., polar
250 regions with strong seasonal temperature variation). Thus, future investigations should be
251 conducted to verify the EIE temperature dependence.

252

253 3.2. Kinetic isotopic fractionation of Leighton Cycle

254 The photochemical reactions of NO_x will compete with the isotope exchange fractionations
255 between NO and NO₂. The NO-NO₂ photochemical cycle in the chamber was controlled by the
256 Leighton cycle: NO₂ photolysis and the NO + O₃ reaction. This is because there were no VOCs in
257 the chamber so no RO₂ was produced, which excludes the NO + RO₂ reaction. Likewise, the low
258 water vapor content (RH<10%) and the minor flux of photons < 310 nm results in minimal OH
259 production and hence little HO₂ formation and subsequently trivial amount of NO₂ would be

Deleted: $\epsilon(\text{NO}_2\text{-NO})$

Deleted: .

Deleted: ‰

Deleted: 2.0

Deleted: ‰

Deleted: .

Deleted: .

Deleted: ‰

Deleted: .

Deleted: .

Deleted: ‰

Deleted: .

Deleted: .

Deleted: ‰

Deleted: 6.7‰

275 formed by NO + HO₂. Applying these limiting assumptions, the EIE between NO and NO₂ (R1-
 276 R2) were only competing with the KIE (R3-R4) and the PHIFE in R5-R6:



281 In which $j(\text{NO}_2)$ is the NO₂ photolysis rate ($1.4 \times 10^{-3} \text{ s}^{-1}$ in these experiments), k_5 is the rate constant
 282 for the NO+O₃ reaction ($1.73 \times 10^{-14} \text{ cm}^3 \text{ s}^{-1}$, Atkinson et al., 2004), and $\alpha_{1,2}$ are isotopic
 283 fractionation factors for the two reactions. Previous studies (Freyer et al., 1993; Walters et al.,
 284 2016) have attempted to assess the competition between EIE (R1-R2), KIE and PHIFE (R3-R6),
 285 but none of them quantified the relative importance of the two processes, nor were α_1 or α_2 values
 286 experimentally determined. Here we provide the mathematical solution of EIE, KIE and PHIFE to
 287 illustrate how R1-R6 affect the isotopic fractionations between NO and NO₂.

288 First, the NO₂ lifetime with respect to isotopic exchange with NO (τ_{exchange}) and photolysis
 289 (τ_{photo}) was determined:

290
$$\tau_{\text{exchange}} = \frac{1}{k_1[\text{NO}]}$$
 Eq. (4)

291
$$\tau_{\text{photo}} = \frac{1}{j(\text{NO}_2)}$$
 Eq. (5)

292 We then define an A factor:

293
$$A = \begin{cases} \frac{\tau_{\text{exchange}}}{\tau_{\text{photo}}} & \text{when } j(\text{NO}_2) \neq 0 \\ 0 & \text{when } j(\text{NO}_2) = 0 \end{cases}$$
 Eq. (6)

Deleted:)x

Deleted: x

Deleted: x

297 Using R1-R6 and Eq. (1)-(6), we solved steady-state $\delta(\text{NO}_2)$ and $\delta(\text{NO})$ values (see calculations
 298 in [Appendix C](#)). Our calculations show that the $\delta(\text{NO}_2)$ - $\delta(\text{NO})$ and $\delta(\text{NO}_2)$ - $\delta(\text{NO}_x)$ values at steady
 299 state can be expressed as functions of α_1 , α_2 , $\alpha(\text{NO}_2\text{-NO})$ and A:

$$\delta(\text{NO}_2) - \delta(\text{NO}) = \frac{(\alpha_2 - \alpha_1) A + (\alpha(\text{NO}_2\text{-NO}) - 1)}{A + 1} (1 + \delta(\text{NO})) \quad \text{Eq. (7)}$$

$$\delta(\text{NO}_2) - \delta(\text{NO}_x) = \frac{(\alpha_2 - \alpha_1) A + (\alpha(\text{NO}_2\text{-NO}) - 1)}{A + 1} (1 + \delta(\text{NO})) (1 - f(\text{NO}_2)) \quad \text{Eq. (8)}$$

300 Equation (7) shows the isotopic fractionation between NO and NO₂ ($\delta(\text{NO}_2)$ - $\delta(\text{NO})$) is determined
 301 by A, the EIE factor ($\alpha(\text{NO}_2\text{-NO})$ -1) and the $(\alpha_2 - \alpha_1)$ factor **assuming $(1 + \delta(\text{NO}))$ is close to 1**. This
 302 $(\alpha_2 - \alpha_1)$ represents a combination of KIE and PHIFE, suggesting they act together as one factor;
 303 therefore, we name the $(\alpha_2 - \alpha_1)$ factor Leighton Cycle Isotopic Effect, i.e., LCIE. Using measured
 304 $(\delta(\text{NO}_2) - \delta(\text{NO})) / (1 + \delta(\text{NO}))$ values, A values, and the previously determined EIE factor, we
 305 calculated that the best fit for the LCIE factor was $(-10 \pm 5) \text{‰}$ (showing the lowest Rooted Mean
 306 Square Error, RMSE, of 1.1‰, Fig. 1C). The uncertainties in the LCIE factor are relatively higher
 307 than that of the EIE factor, mainly because of the accumulated analytical uncertainties at low NO_x
 308 and O₃ concentrations, and low A values (0.10-0.28) due to the relatively low $j(\text{NO}_2)$ value
 309 ($1.4 \times 10^{-3} \text{ s}^{-1}$) under the chamber irradiation conditions.

310 This LCIE factor determined in our experiments is in good agreement with theoretical
 311 calculations. Walters and Michalski (2016) previously used an *ab initio* approach to determine an
 312 α_2 value of 0.9933 at room temperature, 0.9943 at 237 K and 0.9929 at 310 K. The **total** variation
 313 of α_2 values from 273 K to 310 K is only **1.4 ‰**, significantly smaller than our experimental
 314 uncertainty (**$\pm 5 \text{‰}$**). The α_1 value was calculated using a ZPE shift model (Miller & Yung, 2000)
 315 to calculate the isotopic fractionation of NO₂ by photolysis. Briefly, this model assumes both
 316 isotopologues have the same quantum yield function and the PHIFE was only caused by the
 317 differences in the ¹⁵NO₂ and ¹⁴NO₂ absorption cross-section as a function of wavelength, thus α_1
 318
 319

Deleted: supplementary material

Deleted: (‰)

Deleted: ×

Deleted: × 1000 ‰

Deleted: (‰)

Deleted: ×

Deleted: ×

Deleted: × 1000 ‰

Deleted: largely

Deleted: ±0.7

330 values do not vary by temperature. The $^{15}\text{NO}_2$ absorption cross-section was calculated by shifting
331 the $^{14}\text{NO}_2$ absorption cross-section by the $^{15}\text{NO}_2$ zero-point energy (Michalski et al., 2004). When
332 the ZPE shift model was used with the irradiation spectrum of the chamber lights, the resulting α_1
333 value was 1.0023. Therefore, the theoretically predicted $\alpha_2-\alpha_1$ value should be -0.0090, i.e., (-
334 9.0 ± 0.7) ‰ when temperature ranges from 273 K to 310 K. This result shows excellent agreement
335 with our experimentally determined room temperature $\alpha_2-\alpha_1$ value of (- 10 ± 5) ‰.

336 This model was then used to evaluate the variations of α_1 value to different lighting
337 conditions. The TUV model (TUV5.3.2, Madronich & Flocke, 1999) was used to calculate the
338 solar wavelength spectrum at three different conditions: early morning/late afternoon (solar zenith
339 angle=85 degree), mid-morning/afternoon (solar zenith angle=45 degree), noon (solar zenith
340 angle=0 degree). These spectrums were used in the ZPE shift model to calculate the α_1 values,
341 which are 1.0025, 1.0028, and 1.0029 at solar zenith angles of 85, 45 and 0 degree, respectively.
342 These values, along with the predicted α_1 value in the chamber, showed a total span of 0.6‰
343 (1.0026 ± 0.0003), which is again significantly smaller than our measured uncertainty. Therefore,
344 we suggest that our experimentally determined LCIE factor ((- 10 ± 5) ‰) can be used in most
345 tropospheric solar irradiation spectrums.

346 The equations can also be applied in tropospheric environments to calculate the combined
347 isotopic fractionations of EIE and LCIE for NO and NO_2 . First, the NO_2 sink reactions (mainly
348 NO_2+OH in the daytime) are at least 2-3 orders of magnitude slower than the Leighton cycle and
349 the NO- NO_2 isotope exchange reactions (Walters et al., 2016), therefore their effects on the $\delta(\text{NO}_2)$
350 should be minor. Second, although the conversion of NO into NO_2 in the ambient environment is
351 also controlled by $\text{NO} + \text{RO}_2$ and HO_2 in addition to $\text{NO}+\text{O}_3$ (e.g., King et al., 2001), Eq. (7) still
352 showed good agreement with field observations in previous studies. Freyer et al. (1993)

Deleted:

354 determined the annual average daytime $\delta(\text{NO}_2)-\delta(\text{NO})$ at Julich, Germany along with average
355 daytime NO concentration (9 nmol mol^{-1} , similar to our experimental conditions) to be
356 $(+18.03 \pm 0.98) \text{ ‰}$. Using Eq. (7), assuming the daytime average $j(\text{NO}_2)$ value throughout the year
357 was $(5.0 \pm 1.0) \times 10^{-3}$, and a calculated A value from measured NO_x concentration ranged from 0.22-
358 0.33, the average NO- NO_2 fractionation factor was calculated to be $(+18.8 \pm 1.4) \text{ ‰}$ (Fig. 1C), in
359 excellent agreement with the measurements in the present study. This agreement suggests the
360 NO+ RO_2/HO_2 reactions might have similar fractionation factors as NO+ O_3 . Therefore, we suggest
361 Eq. (7) and (8) can be used to estimate the isotopic fractionations between NO and NO_2 in the
362 troposphere.

363

364 3.3 Calculating nitrogen isotopic fractionations of NO- NO_2

365 First, Eq. (7) was used to calculate the $\Delta(\text{NO}_2-\text{NO}) = \delta(\text{NO}_2)-\delta(\text{NO})$ at a wide range of
366 NO_x concentrations, $f(\text{NO}_2)$ and $j(\text{NO}_2)$ values (Fig. 2A-D), assuming $(1+\delta(\text{NO}))=1$. $j(\text{NO}_2)$
367 values of 0 s^{-1} (Fig. 2A), $1.4 \times 10^{-3} \text{ s}^{-1}$ (Fig. 2B), $5 \times 10^{-3} \text{ s}^{-1}$ (Fig. 2C) and $1 \times 10^{-2} \text{ s}^{-1}$ (Fig. 2D) were
368 selected to represent nighttime, dawn (as well as the laboratory conditions of our experiments),
369 daytime average and noon, respectively. Each panel represented a fixed $j(\text{NO}_2)$ value, and the
370 $\Delta(\text{NO}_2-\text{NO})$ values were calculated as a function of the A value, which was derived from NO_x
371 concentration and $f(\text{NO}_2)$. The A values have a large span, from 0 to 500, depending on the $j(\text{NO}_2)$
372 value and the NO concentration. When $A=0$ ($j(\text{NO}_2)=0$) and $f(\text{NO}_2)<1$ (meaning NO- NO_2 coexist
373 and $[\text{O}_3]=0$), Eq. (7) and (8) become Eq. (2) and (3), showing the EIE was the sole factor, the
374 $\Delta(\text{NO}_2-\text{NO})$ values were solely controlled by EIE which has a constant value of $+27.5 \text{ ‰}$ at 298K
375 (Fig. 2A). When $j(\text{NO}_2)>0$, the calculated $\Delta(\text{NO}_2-\text{NO})$ values showed a wide range from -10.0 ‰
376 (controlled by LCIE factor: $\alpha_2-\alpha_1=-10 \text{ ‰}$) to $+27.5 \text{ ‰}$ (controlled by EIE factor: $\alpha(\text{NO}_2-\text{NO})-1 =$

377 +27.5 ‰). Fig. 2B-D display the transition from a LCIE-dominated regime to an EIE-dominated
378 regime. The LCIE-dominated regime is characterized by low $[\text{NO}_x]$ ($<50 \text{ pmol mol}^{-1}$), representing
379 remote ocean areas and polar regions (Beine et al., 2002; Custard et al., 2015). At this range the A
380 value can be greater than 200, thus Eq. (7) can be simplified as: $\Delta(\text{NO}_2\text{-NO}) = \alpha_2 - \alpha_1$, suggesting
381 the LCIE almost exclusively controls the NO-NO₂ isotopic fractionation. The $\Delta(\text{NO}_2\text{-NO})$ values
382 of these regions are predicted to be $<0 \text{ ‰}$ during most time of the day and $< -5 \text{ ‰}$ at noon. On the
383 other hand, the EIE-dominated regime was characterized by high $[\text{NO}_x]$ ($>20 \text{ nmol mol}^{-1}$) and low
384 $f(\text{NO}_2)$ (< 0.6), representative of regions with intensive NO emissions, e.g., near roadside or stack
385 plumes (Clapp & Jenkin, 2001; Kimbrough et al., 2017). In this case, the τ_{exchange} are relatively
386 short (10-50 s) compared to the τ_{photo} (approximately 100 s at noon and 1000 s at dawn), therefore
387 the A values are small (0.01-0.5). The EIE factor in this regime thus is much more important than
388 the LCIE factor, resulting in high $\Delta(\text{NO}_2\text{-NO})$ values ($>20 \text{ ‰}$). Between the two regimes, both
389 EIE and LCIE are competitive and therefore it is necessary to use Eq. (7) to quantify the $\Delta(\text{NO}_2\text{-}$
390 NO) values.

391 Fig. 2 also implies that changes in the $j(\text{NO}_2)$ value can cause the diurnal variations in
392 $\Delta(\text{NO}_2\text{-NO})$ values. Changing $j(\text{NO}_2)$ would affect the value of A and consequently the NO-NO₂
393 isotopic fractionations in two ways: 1) changes in $j(\text{NO}_2)$ value would change the photolysis
394 intensity, therefore the τ_{photo} value; 2) in addition, changes in $j(\text{NO}_2)$ value would also alter the
395 steady state NO concentration, therefore changing the τ_{exchange} (Fig. 2C). The combined effect of
396 these two factors on the A value varies along with the atmospheric conditions, and thus needs to
397 be carefully calculated using NO_x concentration data and atmospheric chemistry models.

398 We then calculated the differences of $\delta^{15}\text{N}$ values between NO₂ and total NO_x, e.g. $\Delta(\text{NO}_2\text{-}$
399 NO_x) = $\delta(\text{NO}_2) - \delta(\text{NO}_x)$ in Fig. 2E-H. Since $\Delta(\text{NO}_2\text{-NO}_x)$ are connected through the observed $\delta^{15}\text{N}$

Deleted: (

Deleted:) $\times 1000 \text{ ‰}$

402 of NO₂ (or nitrate) to the δ¹⁵N of NO_x sources, this term might be useful in field studies (e.g.,
403 Chang et al., 2018; Zong et al., 2017). The calculated Δ(NO₂-NO_x) values (Fig. 2E-H) also showed
404 a LCIE-dominated regime at low [NO_x] and an EIE-dominated regime at high [NO_x]. The Δ(NO₂-
405 NO_x) values were dampened by the 1-*f*(NO₂) factor comparing to Δ(NO₂-NO), as shown in Eq.
406 (3) and (8): Δ(NO₂-NO_x) = Δ(NO₂-NO)(1-*f*(NO₂)). At high *f*(NO₂) values (>0.8), the differences
407 between δ(NO₂) and δ(NO_x) were less than 5 ‰, thus the measured δ(NO₂) values were similar to
408 δ(NO_x), although the isotopic fractionation between NO and NO₂ could be noteworthy. Some
409 ambient environments with significant NO emissions or high NO₂ photolysis rates usually have
410 *f*(NO₂) values between 0.4-0.8 (Mazzeo et al., 2005; Vicars et al., 2013). In this scenario, the
411 Δ(NO₂-NO_x) values in Fig. 2F-H showed wide ranges of -4.8 ‰ to +15.6 ‰, -6.0 ‰ to +15.0 ‰,
412 and -6.3 ‰ to +14.2 ‰ at *j*(NO₂)=1.4×10⁻³ s⁻¹, 5×10⁻³ s⁻¹, 1×10⁻² s⁻¹, respectively. These significant
413 differences again highlighted the importance of both LCIE and EIE (Eq. (7) and (8)) in calculating
414 the Δ(NO₂-NO_x). In the following discussion, we assume 1) the α₁ value remain constant (see
415 discussion above), 2) the NO+RO₂/HO₂ reactions have the same fractionation factors (α₂) as
416 NO+O₃, and 3) both EIE and LCIE do not display significant temperature dependence, then use
417 Equations (7) and (8) and this laboratory determined LCIE factor (-10 ‰) to calculate the nitrogen
418 isotopic fractionation between NO and NO₂ at various tropospheric atmospheric conditions.

419

420 4. Implications

421 The daily variations of Δ(NO₂-NO_x) values at two roadside NO_x monitoring sites were
422 predicted to demonstrate the effects of NO_x concentrations to the NO-NO₂ isotopic fractionations.
423 Hourly NO and NO₂ concentrations were acquired from a roadside site at Anaheim, CA
424 (<https://www.arb.ca.gov>) and an urban site at Evansville, IN (<http://idem.tx.sutron.com>) on July

Deleted: x

426 25, 2018. The hourly $j(\text{NO}_2)$ values output from the TUV model (Madronich & Flocke, 1999) at
427 these locations was used to calculate the daily variations of $\Delta(\text{NO}_2\text{-NO}_x)$ values (Fig. 3A, B) by
428 applying Eq. (8) and assuming $(1+\delta(\text{NO}))=1$. Hourly NO_x concentrations were 12-51 nmol mol^{-1}
429 at Anaheim and 9-38 nmol mol^{-1} at Evansville and the $f(\text{NO}_2)$ values at both sites did not show
430 significant daily variations (0.45 ± 0.07 at Anaheim and 0.65 ± 0.08 at Evansville), likely because
431 the NO_x concentrations were controlled by the high NO emissions from the road (Gao, 2007). The
432 calculated $\Delta(\text{NO}_2\text{-NO}_x)$ values using Eq. (8) showed significant diurnal variations. During the
433 nighttime, the isotopic fractionations were solely controlled by the EIE, the predicted $\Delta(\text{NO}_2\text{-NO}_x)$
434 values were $(+14.5\pm 2.0)$ ‰ and $(+8.7\pm 2.1)$ ‰ at Anaheim and Evansville, respectively. During
435 the daytime, the existence of LCIE lowered the predicted $\Delta(\text{NO}_2\text{-NO}_x)$ values to $(+9.8\pm 1.7)$ ‰ at
436 Anaheim and $(+3.1\pm 1.5)$ ‰ at Evansville while the $f(\text{NO}_2)$ values at both sites remained similar.
437 The lowest $\Delta(\text{NO}_2\text{-NO}_x)$ values for both sites ($+7.0$ ‰ and $+1.7$ ‰) occurred around noon when
438 the NO_x photolysis was the most intense. In contrast, if one neglects the LCIE factor in the daytime,
439 the $\Delta(\text{NO}_2\text{-NO}_x)$ values would be $(+12.9\pm 1.5)$ ‰ and $(+10.0\pm 1.6)$ ‰ respectively, an
440 overestimation of 3.1 ‰ and 6.9 ‰. These discrepancies suggested that the LCIE played an
441 important role in the $\text{NO}\text{-NO}_2$ isotopic fractionations and neglecting it could bias the NO_x source
442 apportionment using $\delta^{15}\text{N}$ of NO_2 or nitrate.

443 The role of LCIE was more important in less polluted sites. The $\Delta(\text{NO}_2\text{-NO}_x)$ values
444 calculated for a suburban site near San Diego, CA, USA, again using the hourly NO_x
445 concentrations (<https://www.arb.ca.gov>, Fig. 3C) and $j(\text{NO}_2)$ values calculated from the TUV
446 model. NO_x concentrations at this site varied from 1 to 9 nmol mol^{-1} and assuming $(1+\delta(\text{NO}))=1$.
447 During the nighttime, NO_x was in the form of NO_2 ($f(\text{NO}_2) = 1$) because O_3 concentrations were
448 higher than NO_x , thus the $\delta(\text{NO}_2)$ values should be identical to $\delta(\text{NO}_x)$ ($\Delta(\text{NO}_2\text{-NO}_x) = 0$). In the

449 daytime a certain amount of NO was produced by direct NO emission and NO₂ photolysis but the
450 $f(\text{NO}_2)$ was still high (0.73 ± 0.08). Our calculation suggested the daytime $\Delta(\text{NO}_2\text{-NO}_x)$ values
451 should be only $(+1.3 \pm 3.2)$ ‰ with a lowest value of -1.3 ‰. These $\Delta(\text{NO}_2\text{-NO}_x)$ values were
452 similar to the observed and modeled summer daytime $\delta(\text{NO}_2)$ values in West Lafayette, IN
453 (Walters et al., 2018), which suggest the average daytime $\Delta(\text{NO}_2\text{-NO}_x)$ values at $\text{NO}_x = (3.9 \pm 1.2)$
454 nmol mol^{-1} should range from +0.1 ‰ to +2.4 ‰. In this regime, we suggest the $\Delta(\text{NO}_2\text{-NO}_x)$
455 values were generally small due to the significant contribution of LCIE and high $f(\text{NO}_2)$.

456 The LCIE should be the dominant factor controlling the NO-NO₂ isotopic fractionation at
457 remote regions, resulting in a completely different diurnal pattern of $\Delta(\text{NO}_2\text{-NO}_x)$ compared with
458 the urban-suburban area. Direct hourly measurements of NO_x at remote sites are rare, thus we used
459 total NO_x concentration of 50 pmol mol^{-1} , daily O₃ concentration of 20 nmol mol^{-1} at Summit,
460 Greenland (Dibb et al., 2002; Hastings et al., 2004; Honrath et al., 1999; Yang et al., 2002), and
461 assumed $(1 + \delta(\text{NO})) = 1$ and the conversion of NO to NO₂ was completely controlled by O₃ to
462 calculate the NO/NO₂ ratios. Here the isotopes of NO_x were almost exclusively controlled by the
463 LCIE due to the high A values (>110). The $\Delta(\text{NO}_2\text{-NO}_x)$ values displayed a clear diurnal pattern
464 (Fig. 3D) with highest value of -0.3 ‰ in the “nighttime” (solar zenith angle >85 degree) and
465 lowest value of -5.0 ‰ in the mid-day. This suggest that the isotopic fractionations between NO
466 and NO₂ were almost completely controlled by LCIE at remote regions, when NO_x concentrations
467 were <0.1 nmol mol^{-1} . However, since the isotopic fractionation factors of nitrate-formation
468 reactions (NO₂+OH, NO₃+HC, N₂O₅+H₂O) are still unknown, more studies are needed to fully
469 explain the daily and seasonal variations of $\delta(\text{NO}_3^-)$ at remote regions.

470 Nevertheless, our results have a few limitations. First, currently there are very few field
471 observations that can be used to evaluate our model, therefore, future field observations that

472 measure the $\delta^{15}\text{N}$ values of ambient NO and NO_2 should be carried out to test our model. Second,
473 more work, including theoretical and experimental studies, is needed to investigate the isotope
474 fractionation factors occurring during the conversion from NO_x to NO_y and nitrate: in the NO_y
475 cycle, EIE (isotopic exchange between NO_2 , NO_3 and N_2O_5), KIE (formation of NO_3 , N_2O_5 and
476 nitrate) and PHIFE (photolysis of NO_3 , N_2O_5 , HONO and sometimes nitrate) may also exist and
477 be relevant for the $\delta^{15}\text{N}$ of HNO_3 and HONO. In particular, the N isotope fractionation occurring
478 during the $\text{NO}_2 + \text{OH} \rightarrow \text{HNO}_3$ reaction needs investigation. Such studies could help us modeling
479 the isotopic fractionation between NO_x emission and nitrate, and eventually enable us to analyze
480 the $\delta^{15}\text{N}$ value of NO_x emission by measuring the $\delta^{15}\text{N}$ values of nitrate aerosols and nitrate in wet
481 depositions. Third, our discussion only focuses on the reactive nitrogen chemistry in the
482 troposphere, however, the nitrogen chemistry in the stratosphere is drastically different from the
483 tropospheric chemistry, thus future studies are also needed to investigate the isotopic fractionations
484 in the stratospheric nitrogen chemistry. Last, the temperature dependence of both EIE and LCIE
485 needs to be carefully investigated, because of the wide range of temperature in both troposphere
486 and stratosphere. Changes in temperature could alter the isotopic fractionation factors of both EIE
487 and LCIE, as well as contribute to the seasonality of isotopic fractionations between NO_x and NO_y
488 molecules.

489

490 **5. Conclusions**

491 The effect of NO_x photochemistry on the nitrogen isotopic fractionations between NO and
492 NO_2 was investigated. We first measured the isotopic fractionations between NO and NO_2 and
493 provided mathematical solutions to assess the impact of NO_x level and NO_2 photolysis rate ($j(\text{NO}_2)$)
494 to the relative importance of EIE and LCIE. The EIE and LCIE isotope fractionation factors, at

495 room temperature, were determined to be 1.0275 ± 0.0012 and 0.990 ± 0.005 , respectively. These
496 calculations and measurements can be used to determine the steady state $\Delta(\text{NO}_2\text{-NO})$ and $\Delta(\text{NO}_2\text{-}$
497 $\text{NO}_x)$ values at room temperature. Subsequently we applied our equations to polluted, clean and
498 remote sites to model the daily variations of $\Delta(\text{NO}_2\text{-NO}_x)$ values. We found that the $\Delta(\text{NO}_2\text{-NO}_x)$
499 values could vary from over +20 ‰ to less than -5 ‰ depending on the environment: in general,
500 the role of LCIE becoming more important at low NO_x concentrations, which tend to decrease the
501 $\Delta(\text{NO}_2\text{-NO}_x)$ values. Our work provided a mathematical approach to quantify the nitrogen isotopic
502 fractionations between NO and NO_2 that can be applied to many tropospheric environments, which
503 could help interpret the measured $\delta^{15}\text{N}$ values of NO_2 and nitrate in field observation studies.

504

505 **Acknowledgement**

506 We thank NCAR's Advanced Study Program granted to Jianghanyang Li. The National
507 Center for Atmospheric Research is operated by the University Corporation for Atmospheric
508 Research, under the sponsorship of the National Science Foundation. We also thank funding
509 support from Purdue Climate Change Research Center and A. H. Ismail Interdisciplinary Program
510 Doctoral Research Travel Award granted by Purdue University.

511 **Data Availability**

512 Data acquired from this study was deposited at Open Sciences Framework (Li, 2019,
513 DOI 10.17605/OSF.IO/JW8HU).

514 **Author contribution**

515 J. Li and G. Michalski designed the experiments, X. Zhang and J. Li conducted the
516 experiments. X. Zhang, G. Michalski, J. Orlando and G. Tyndall helped J. Li in interpreting the

517 results. The manuscript was written by J. Li and all the authors have contributed during the revision
518 of this manuscript.

519 **Competing interest**

520 The authors declare no competing interest.

521

522 **References:**

523

524 [Atkinson, R., Baulch, D. L., Cox, R. A., Crowley, J. N., Hampson, R. F., Hynes, R. G., Jenkin, M.](#)
525 [E., Rossi, M. J., and Troe, J. \(2004\). Evaluated kinetic and photochemical data for atmospheric](#)
526 [chemistry: Volume I-gas phase reactions of O_x, HO_x, NO_x and SO_x. Atmospheric chemistry and](#)
527 [physics, 4\(6\), 1461-1738. https://doi.org/10.5194/acp-4-1461-2004, 2004.](#)

528

529 Barney, W. S., & Finlayson-Pitts, B. J. (2000). Enhancement of N₂O₄ on porous glass at room
530 temperature: A key intermediate in the heterogeneous hydrolysis of NO₂? The Journal of Physical
531 Chemistry A, 104(2), 171–175. [https://doi.org/10.1021/jp993169b](#)

532

533 Begun, G. M., & Fletcher, W. H. (1960). Partition function ratios for molecules containing
534 nitrogen isotopes. The Journal of Chemical Physics, 33(4), 1083–1085.
535 [https://doi.org/10.1063/1.1731338](#)

536

537 Begun, G. M., & Melton, C. E. (1956). Nitrogen isotopic fractionation between NO and NO₂ and
538 mass discrimination in mass analysis of NO₂. The Journal of Chemical Physics, 25(6), 1292–1293.
539 [https://doi.org/10.1063/1.1743215](#)

540

541 Beine, H. J., Honrath, R. E., Dominé, F., Simpson, W. R., & Fuentes, J. D. (2002). NO_x during
542 background and ozone depletion periods at Alert: Fluxes above the snow surface. Journal of
543 Geophysical Research: Atmospheres, 107(D21), ACH-7. [https://doi.org/10.1029/2002JD002082](#)

544

545 Bigeleisen, J., & Mayer, M. G. (1947). Calculation of equilibrium constants for isotopic exchange
546 reactions. The Journal of Chemical Physics, 15(5), 261-267. [https://doi.org/10.1063/1.1746492](#)

547

548 Bigeleisen, J., & Wolfsberg, M. (1957). Theoretical and experimental aspects of isotope effects in
549 chemical kinetics. Advances in Chemical Physics, 15–76.
550 [https://doi.org/10.1002/9780470143476.ch2](#)

551

552 Casciotti, K. L., & McIlvin, M. R. (2007). Isotopic analyses of nitrate and nitrite from reference
553 mixtures and application to Eastern Tropical North Pacific waters. Marine Chemistry, 107(2), 184–
554 201. [https://doi.org/10.1016/j.marchem.2007.06.021](#)

555

556 Chang, Y., Zhang, Y., Tian, C., Zhang, S., Ma, X., Cao, F., et al. (2018). Nitrogen isotope
557 fractionation during gas-to-particle conversion of NO_x to NO₃⁻ in the atmosphere—implications for

Formatted: Subscript

Formatted: Subscript

Formatted: Subscript

Formatted: Subscript

Deleted: Atkinson, R., Baulch, D. L., Cox, R. A., Crowley, J. N., Hampson, R. F., Hynes, R. G., et al. (2004). Evaluated kinetic and photochemical data for atmospheric chemistry: Volume I-gas phase reactions of O_x, HO_x, NO_x and SO_x species. Atmospheric Chemistry and Physics, 4(6), 1461–1738.

564 isotope-based NO_x source apportionment. *Atmospheric Chemistry and Physics*, 18(16), 11647–
565 11661. <https://doi.org/10.5194/acp-18-11647-2018>, 2018.
566

567 Clapp, L. J., & Jenkin, M. E. (2001). Analysis of the relationship between ambient levels of O₃,
568 NO₂ and NO as a function of NO_x in the UK. *Atmospheric Environment*, 35(36), 6391–6405.
569 [https://doi.org/10.1016/S1352-2310\(01\)00378-8](https://doi.org/10.1016/S1352-2310(01)00378-8)
570

571 [Custard, K. D., Thompson, C. R., Pratt, K. A., Shepson, P. B., Liao, J., Huey, L. G., Orlando, J. J.,
572 Weinheimer, A. J., Apel, E., Hall, S. R., Flocke, F., Mauldin, L., Hornbrook, R. S., Pöhler, D.,
573 General, S., Zielcke, J., Simpson, W. R., Platt, U., Fried, A., Weibring, P., Sive, B. C., Ullmann,
574 K., Cantrell, C., Knapp, D. J., and Montzka, D. D.: The NO_x dependence of bromine chemistry in
575 the Arctic atmospheric boundary layer, *Atmos. Chem. Phys.*, 15, 10799–10809,
576 <https://doi.org/10.5194/acp-15-10799-2015>, 2015.](https://doi.org/10.5194/acp-15-10799-2015)
577

578 Dibb, J. E., Arsenault, M., Peterson, M. C., & Honrath, R. E. (2002). Fast nitrogen oxide
579 photochemistry in Summit, Greenland snow. *Atmospheric Environment*, 36(15–16), 2501–2511.
580 [https://doi.org/10.1016/S1352-2310\(02\)00130-9](https://doi.org/10.1016/S1352-2310(02)00130-9)
581

582 Do Remus, R. H., Mehrotra, Y., Lanford, W. A., & Burman, C. (1983). Reaction of water with
583 glass: influence of a transformed surface layer. *Journal of Materials Science*, 18(2), 612–622.
584 <https://doi.org/10.1007/BF00560651>
585

586 [Elliott, E. M., Kendall, C., Boyer, E. W., Burns, D. A., Lear, G. G., Golden, H. E., Harlin, K.,
587 Bytnerowicz, A., Butler, T. J., and Glatz, R. \(2009\). Dual nitrate isotopes in dry deposition: Utility
588 for partitioning NO_x source contributions to landscape nitrogen deposition. *Journal of Geophysical
589 Research: Biogeosciences*, 114\(G4\), G04020. <https://doi.org/10.1029/2008JG000889>
590](https://doi.org/10.1029/2008JG000889)

591 Felix, J. D., & Elliott, E. M. (2014). Isotopic composition of passively collected nitrogen dioxide
592 emissions: Vehicle, soil and livestock source signatures. *Atmospheric Environment*, 92, 359–366.
593 <https://doi.org/10.1016/j.atmosenv.2014.04.005>
594

595 Felix, J. D., Elliott, E. M., & Shaw, S. L. (2012). Nitrogen isotopic composition of coal-fired power
596 plant NO_x: influence of emission controls and implications for global emission inventories.
597 *Environmental Science & Technology*, 46(6), 3528–3535. <https://doi.org/10.1021/es203355v>
598

599 Frey, M. M., Savarino, J., Morin, S., Erbland, J., & Martins, J. M. F. (2009). Photolysis imprint in
600 the nitrate stable isotope signal in snow and atmosphere of East Antarctica and implications for
601 reactive nitrogen cycling. *Atmos. Chem. Phys.*, 9, 8681–8696. [https://doi.org/10.5194/acp-9-8681-
2009](https://doi.org/10.5194/acp-9-8681-
602 2009), 2009.
603

604 Freyer, H. D. (1991). Seasonal variation of ¹⁵N/¹⁴N ratios in atmospheric nitrate species. *Tellus B*,
605 43(1), 30–44. <https://doi.org/10.1034/j.1600-0889.1991.00003.x>
606

607 Freyer, H. D., Kley, D., Volz-Thomas, A., & Kobel, K. (1993). On the interaction of isotopic
608 exchange processes with photochemical reactions in atmospheric oxides of nitrogen. *Journal of
609 Geophysical Research: Atmospheres*, 98(D8), 14791–14796. <https://doi.org/10.1029/93JD00874>

Deleted: Custard, K. D., Thompson, C. R., Pratt, K. A., Shepson, P. B., Liao, J., Huey, L. G., et al. (2015). The NO_x dependence of bromine chemistry in the Arctic atmospheric boundary layer. *Atmospheric Chemistry and Physics*, 15(18), 10799–10809.

Deleted: Elliott, E. M., Kendall, C., Boyer, E. W., Burns, D. A., Lear, G. G., Golden, H. E., et al. (2009).

617
618 Gao, H. O. (2007). Day of week effects on diurnal ozone/NO_x cycles and transportation emissions
619 in Southern California. *Transportation Research Part D: Transport and Environment*, 12(4), 292–
620 305. <https://doi.org/10.1016/j.trd.2007.03.004>
621
622 Gobel, A. R., Altieri, K. E., Peters, A. J., Hastings, M. G., & Sigman, D. M. (2013). Insights into
623 anthropogenic nitrogen deposition to the North Atlantic investigated using the isotopic
624 composition of aerosol and rainwater nitrate. *Geophysical Research Letters*, 40(22), 5977–5982.
625 <https://doi.org/10.1002/2013GL058167>
626
627 Hastings, M G, Jarvis, J. C., & Steig, E. J. (2009). Anthropogenic impacts on nitrogen isotopes of
628 ice-core nitrate. *Science*, 324(5932), 1288. DOI: [10.1126/science.1170510](https://doi.org/10.1126/science.1170510)
629
630 Hastings, M G, Steig, E. J., & Sigman, D. M. (2004). Seasonal variations in N and O isotopes of
631 nitrate in snow at Summit, Greenland: Implications for the study of nitrate in snow and ice cores.
632 *Journal of Geophysical Research: Atmospheres*, 109(D20).
633 <https://doi.org/10.1029/2004JD004991>,
634
635 Honrath, R. E., Peterson, M. C., Guo, S., Dibb, J. E., Shepson, P. B., & Campbell, B. (1999).
636 Evidence of NO_x production within or upon ice particles in the Greenland snowpack. *Geophysical*
637 *Research Letters*, 26(6), 695–698. <https://doi.org/10.1029/1999GL900077>
638
639 Jarvis, J. C., Steig, E. J., Hastings, M. G., & Kunasek, S. A. (2008). Influence of local
640 photochemistry on isotopes of nitrate in Greenland snow. *Geophysical Research Letters*, 35(21).
641 <https://doi.org/10.1029/2008GL035551>
642
643 Kendall, C., Elliott, E. M., & Wankel, S. D. (2007). Tracing anthropogenic inputs of nitrogen to
644 ecosystems. *Stable Isotopes in Ecology and Environmental Science*, 2, 375–449.
645 <https://doi.org/10.1002/9780470691854.ch12>
646
647 Kimbrough, S., Owen, R. C., Snyder, M., & Richmond-Bryant, J. (2017). NO to NO₂ conversion
648 rate analysis and implications for dispersion model chemistry methods using Las Vegas, Nevada
649 near-road field measurements. *Atmospheric Environment*, 165, 23–34.
650 <https://doi.org/10.1016/j.atmosenv.2017.06.027>
651
652 King, M. D., Canosa-Mas, C. E. and Wayne R. P. (2001). Gas-phase reactions between RO₂ and
653 NO, HO₂ or CH₃O₂: correlations between rate constants and the SOMO energy of the peroxy (RO₂)
654 radical. *Atmospheric Environment* 35.12 (2001): 2081-2088. [https://doi.org/10.1016/S1352-
655 2310\(00\)00501-X](https://doi.org/10.1016/S1352-2310(00)00501-X)
656
657 [Knote, C., Tuccella, P., Curci, G., Emmons, L., Orlando, J. J. Madronich, S., Baró, R., Jiménez-
658 Guerrero, P., Luecken, D., Hogrefe, C., Forkel, R., Werhahn, J., Hirtl, M., Pérez, J. L., San José,
659 R., Giordano, L., Brunner, D., Yahya, K., Zhang, Y., Influence of the choice of gas-phase
660 mechanism on predictions of key gaseous pollutants during the AQMEII phase-2 intercomparison,](#)
661 *Atmospheric Environment* 115 (2015): 553-568. <https://doi.org/10.1016/j.atmosenv.2014.11.066>.
662

Deleted: ¶

Deleted: Hoefs, J. (2009). *Stable isotope geochemistry* (Vol. 285). Springer.¶

Deleted: Martin

Deleted: Carlos E.

Deleted: Richard P.

Deleted: .

Deleted: "

Deleted: "

Deleted: Knote, Christoph,

Deleted: et al. "

Deleted: "

675 Li, J. (2019). Quantifying the nitrogen equilibrium and photochemistry-induced kinetic isotopic
676 effects between NO and NO₂. Retrieved from osf.io/jw8hu
677
678 Madronich, S., & Flocke, S. (1999). The role of solar radiation in atmospheric chemistry. In
679 Environmental photochemistry (pp. 1–26). *The Handbook of Environmental Chemistry (Reactions
680 and Processes), vol 2 / 2L*. Springer, Berlin, Heidelberg, [https://doi.org/10.1007/978-3-540-69044-
681 3_1](https://doi.org/10.1007/978-3-540-69044-3_1)
682
683 Mazzeo, N. A., Venegas, L. E., & Choren, H. (2005). Analysis of NO, NO₂, O₃ and NO_x
684 concentrations measured at a green area of Buenos Aires City during wintertime. Atmospheric
685 Environment, 39(17), 3055–3068. <https://doi.org/10.1016/j.atmosenv.2005.01.029>
686
687 McIlvin, M. R., & Altabet, M. A. (2005). Chemical conversion of nitrate and nitrite to nitrous
688 oxide for nitrogen and oxygen isotopic analysis in freshwater and seawater. Analytical Chemistry,
689 77(17), 5589–5595. <https://doi.org/10.1021/ac050528s>
690
691 Michalski, G., Jost, R., Sugny, D., Joyeux, M., & Thiemens, M. (2004). Dissociation energies of
692 six NO₂ isotopologues by laser induced fluorescence spectroscopy and zero-point energy of some
693 triatomic molecules. The Journal of Chemical Physics, 121(15), 7153–7161.
694 <https://doi.org/10.1063/1.1792233>
695
696 Michalski, G., Bockheim, J. G., Kendall, C., & Thiemens, M. (2005). Isotopic composition of
697 Antarctic Dry Valley nitrate: Implications for NO_y sources and cycling in Antarctica. Geophysical
698 Research Letters, 32(13). <https://doi.org/10.1029/2004GL022121>
699
700 Miller, C. E., & Yung, Y. L. (2000). Photo-induced isotopic fractionation. Journal of Geophysical
701 Research: Atmospheres, 105(D23), 29039–29051. <https://doi.org/10.1029/2000JD900388>
702
703 Monse, E. U., Spindel, W., & Stern, M. J. (1969). Analysis of isotope-effect calculations illustrated
704 with exchange equilibria among oxynitrogen compounds. Rutgers-The State Univ., Newark, NJ.
705 DOI: [10.1021/ba-1969-0089.ch009](https://doi.org/10.1021/ba-1969-0089.ch009)
706
707 Morin, S., Savarino, J., Frey, M. M., Domine, F., Jacobi, H.-W., Kaleschke, L., & Martins, J. M.
708 F. (2009). Comprehensive isotopic composition of atmospheric nitrate in the Atlantic Ocean
709 boundary layer from 65°S to 79°N. J. Geophys. Res, 114. <https://doi.org/10.1029/2008JD010696>
710
711 Park, Y.-M., Park, K.-S., Kim, H., Yu, S.-M., Noh, S., Kim, M.-S., Kim, J.-Y., Ahn, J.-Y., Lee,
712 M.-D., Seok, K.-S., Kin, Y.-H., (2018). Characterizing isotopic compositions of TC-C, NO₃-N,
713 and NH₄⁺-N in PM_{2.5} in South Korea: Impact of China's winter heating.
714 <https://doi.org/10.1016/j.envpol.2017.10.072>
715
716 Saliba, N. A., Yang, H., & Finlayson-Pitts, B. J. (2001). Reaction of gaseous nitric oxide with
717 nitric acid on silica surfaces in the presence of water at room temperature. The Journal of Physical
718 Chemistry A, 105(45), 10339–10346. <https://doi.org/10.1021/jp012330r>
719

Deleted: Springer.

Deleted: et al.

722 Savarino, J., Morin, S., Erbland, J., Grannec, F., Patey, M. D., Vicars, W., Alexander, B.,
723 Achterberg, E. P. (2013). Isotopic composition of atmospheric nitrate in a tropical marine
724 boundary layer. *Proceedings of the National Academy of Sciences*, 110(44), 17668–17673.
725 <https://doi.org/10.1073/pnas.1216639110>
726
727 Sharma, H. D., Jervis, R. E., & Wong, K. Y. (1970). Isotopic exchange reactions in nitrogen oxides.
728 *The Journal of Physical Chemistry*, 74(4), 923–933. <https://doi.org/10.1021/j100699a044>
729
730 Takei, T., Yamazaki, A., Watanabe, T., & Chikazawa, M. (1997). Water adsorption properties on
731 porous silica glass surface modified by trimethylsilyl groups. *Journal of Colloid and Interface*
732 *Science*, 188(2), 409–414. <https://doi.org/10.1006/jcis.1997.4777>
733
734 Urey, H. C. (1947). The thermodynamic properties of isotopic substances. *Journal of the Chemical*
735 *Society (Resumed)*, 562–581. <https://doi.org/10.1039/JR9470000562>
736
737 Vicars, W. C., Morin, S., Savarino, J., Wagner, N. L., Erbland, J., Vince, E., Martins, J. M. F.,
738 Lerner, B. M., Quinn, P. K., Coffman, D. J., Williams, E. J., Brown, S. S., (2013). Spatial and
739 diurnal variability in reactive nitrogen oxide chemistry as reflected in the isotopic composition of
740 atmospheric nitrate: Results from the CalNex 2010 field study. *Journal of Geophysical Research:*
741 *Atmospheres*, 118(18), 10–567. <https://doi.org/10.1002/jgrd.50680>
742
743 Walters, W. W., & Michalski, G. (2015). Theoretical calculation of nitrogen isotope equilibrium
744 exchange fractionation factors for various NO_y molecules. *Geochimica et Cosmochimica Acta*,
745 164, 284–297. <https://doi.org/10.1016/j.gca.2015.05.029>
746
747 Walters, W. W., Goodwin, S. R., & Michalski, G. (2015). Nitrogen stable isotope composition
748 ($\delta^{15}\text{N}$) of vehicle-emitted NO_x. *Environmental Science & Technology*, 49(4), 2278–2285.
749 <https://doi.org/10.1021/es505580v>
750
751 Walters, W. W., & Michalski, G. (2016). Ab initio study of nitrogen and position-specific oxygen
752 kinetic isotope effects in the NO+O₃ reaction. *The Journal of chemical physics*, 145(22), 224311.
753 <https://doi.org/10.1063/1.4968562>
754
755 Walters, W. W., Simonini, D. S., & Michalski, G. (2016). Nitrogen isotope exchange between NO
756 and NO₂ and its implications for $\delta^{15}\text{N}$ variations in tropospheric NO_x and atmospheric nitrate.
757 *Geophysical Research Letters*, 43(1), 440–448. <https://doi.org/10.1002/2015GL066438>
758
759 Walters, W. W., Fang, H., & Michalski, G. (2018). Summertime diurnal variations in the isotopic
760 composition of atmospheric nitrogen dioxide at a small midwestern United States city.
761 *Atmospheric Environment*, 179, 1–11. <https://doi.org/10.1016/j.atmosenv.2018.01.047>
762
763 Williams, E. L., & Grosjean, D. (1990). Removal of atmospheric oxidants with annular denuders.
764 *Environmental Science & Technology*, 24(6), 811–814. <https://doi.org/10.1021/es00076a002>
765
766 Yang, J., Honrath, R. E., Peterson, M. C., Dibb, J. E., Sumner, A. L., Shepson, P. B., Frey, M.,
767 Jacobi, H.-W., Swanson, A., Blake, N., (2002). Impacts of snowpack emissions on deduced levels

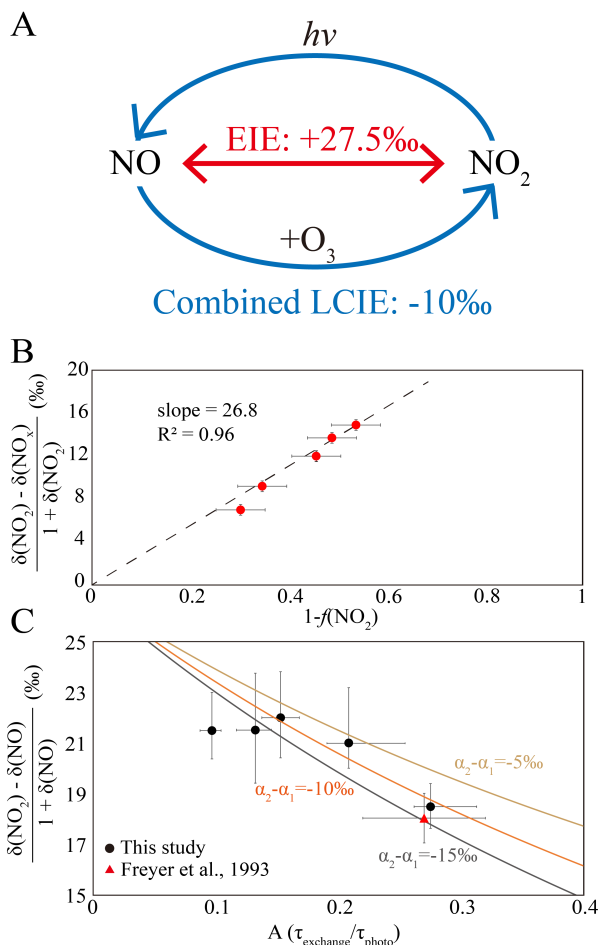
Deleted: et al.

Deleted: et al.

Deleted: et al.

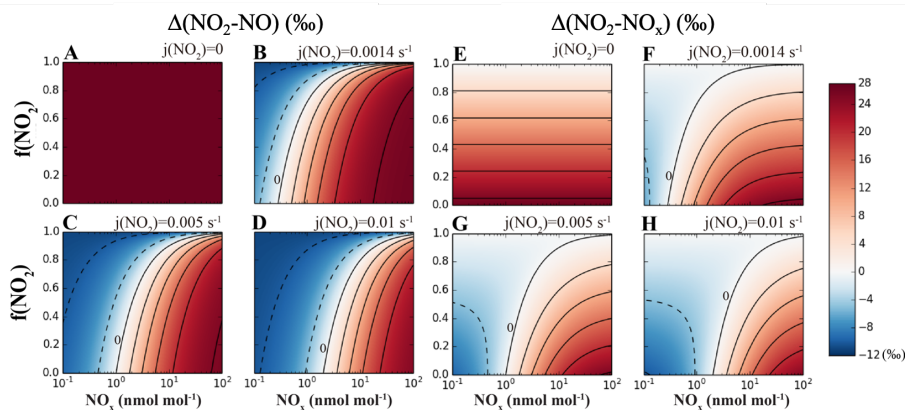
771 of OH and peroxy radicals at Summit, Greenland. *Atmospheric Environment*, 36(15–16), 2523–
772 2534. [https://doi.org/10.1016/S1352-2310\(02\)00128-0](https://doi.org/10.1016/S1352-2310(02)00128-0)
773
774 Zhang, X., Ortega, J., Huang, Y., Shertz, S., Tyndall, G. S., & Orlando, J. J. (2018). A steady-state
775 continuous flow chamber for the study of daytime and nighttime chemistry under atmospherically
776 relevant NO levels. *Atmospheric Measurement Techniques*, 11(5), 2537–2551.
777 <https://doi.org/10.5194/amt-11-2537-2018>
778
779 Zong, Z., Wang, X., Tian, C., Chen, Y., Fang, Y., Zhang, F., ~~Li, C., Sun, J., Li, J., Zhang, G.,~~
780 (2017). First assessment of NO_x sources at a regional background site in North China using
781 isotopic analysis linked with modeling. *Environmental Science & Technology*, 51(11), 5923–5931.
782 <https://doi.org/10.1021/acs.est.6b06316>

Deleted: et al.

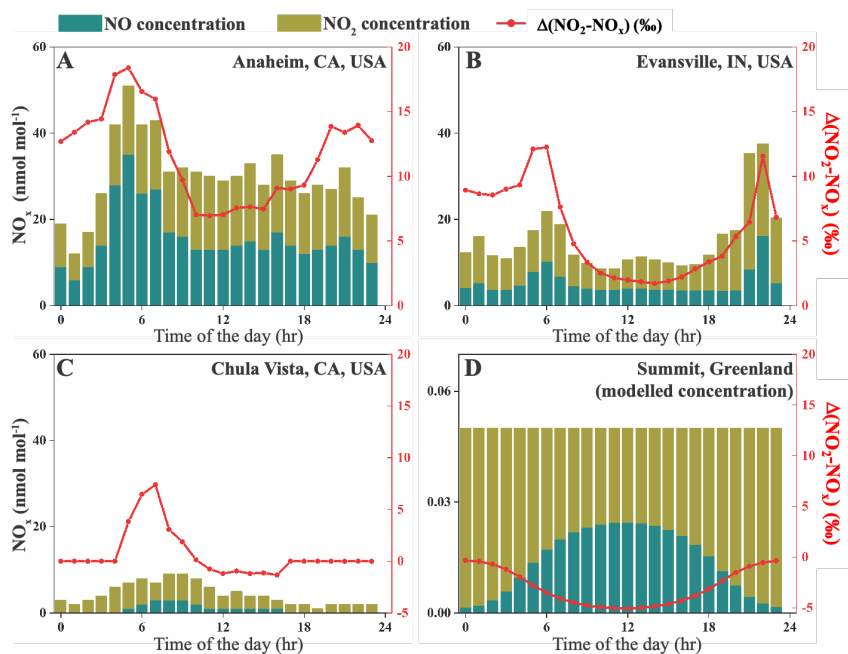


784
 785 **Fig. 1** A. a sketch of the isotopic fractionation processes between NO and NO₂, both fractionation
 786 factors are determined in this work. **B.** Results from five dark experiments yielded a line with slope
 787 of 0.0268 and an $\alpha(\text{NO}_2\text{-NO})$ value of 1.0275. **C.** Results from five UV irradiation experiments
 788 (black points) and a previous field study (red triangle). The three lines represent different $(\alpha_2 - \alpha_1)$
 789 values: the $(\alpha_2 - \alpha_1) = -10\text{‰}$ line showed the lowest RMSE to our experimental data as well as the
 790 previous field observation. The error bars in panels B and C represented the combined uncertainties
 791 of NO_x concentration measurements and isotopic analysis.
 792

- Deleted: $\epsilon(\text{NO}_2\text{-NO})/(1+\epsilon(\text{NO}_2\text{-NO}))$ value
- Deleted: 6.8
- Deleted: ‰
- Deleted: ϵ
- Deleted: .
- Deleted: ‰



799
 800 **Fig. 2** Calculating isotopic fractionation values between NO-NO₂ ($\Delta(\text{NO}_2\text{-NO})$, **A-D**) and NO_x-
 801 NO₂ ($\Delta(\text{NO}_2\text{-NO}_x)$, **E-H**) at various $j(\text{NO}_2)$, NO_x level and $f(\text{NO}_2)$ using Eq. (7) and (8). Each
 802 panel represents a fixed $j(\text{NO}_2)$ value (showing on the upper right side of each panel), and the
 803 fractionation values are shown by color. Lines are contours with the same fractionation values, at
 804 an interval of 5‰, the contour line representing 0‰ was marked on each panel except for A and
 805 E.



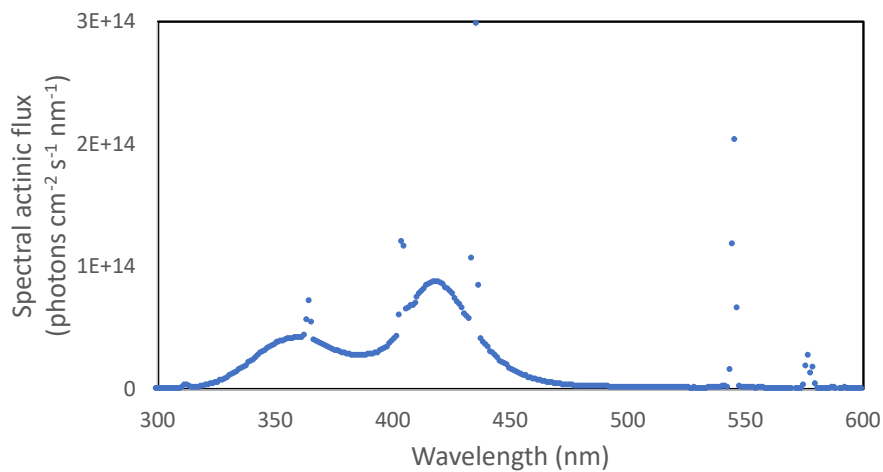
806
 807 **Fig. 3** NO_x concentrations and calculated $\Delta(\text{NO}_2-\text{NO}_x)$ values at four sites. Stacked bars show the
 808 NO and NO₂ concentrations extracted from monitoring sites (A-C) or calculated using 0-D box
 809 model (D); the red lines are $\Delta(\text{NO}_2-\text{NO}_x)$ values at each site. Note that the NO_x concentration (left-
 810 y) axis on panel D is different from the rest.
 811

812 **Appendix A. Chamber descriptions**

813 The chamber is a 10 m³ Teflon bag equipped with several standard instruments including
814 temperature and humidity probe, NO_x monitor and O₃ monitor. 128 wall-mounted blacklight tubes
815 surrounded the chamber to mimic tropospheric photochemistry and the photolysis rate of NO₂
816 ($j(\text{NO}_2)$) when all lights are on have been previously determined to be $1.4 \times 10^{-3} \text{ s}^{-1}$, similar to a
817 $j(\text{NO}_2)$ coefficient at an 81-degree solar zenith angle. The irradiation spectrum of the blacklights
818 are shown in Figure A1. The chamber was kept at room temperature and one atmospheric pressure.
819 Before each experiment, the chamber was flushed with zero air at 40 L min⁻¹ for at least 12 hours
820 to ensure the background NO_x, O₃ and other trace gases were below detection limit.

Formatted: Line spacing: Double
Formatted: Font: Bold

821



822

823 **Figure A1 Spectral actinic flux versus wavelengths of the UV light source used in our experiments.**

824

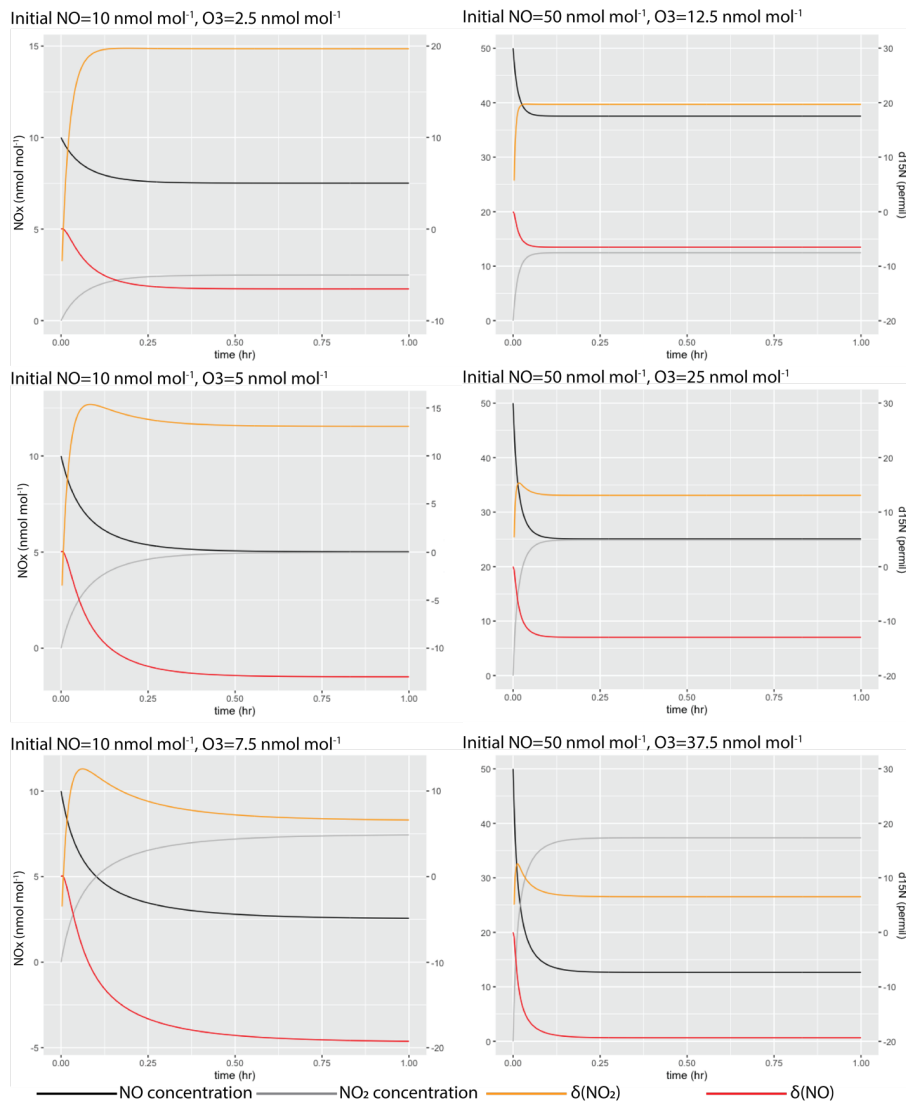
825 **Appendix B. Box model assessing the time needed for NO-NO₂ to reach isotopic equilibrium**

826 The time needed to reach NO-NO₂ isotopic equilibrium during light-off experiments were
827 assessed using a 0-D box model. This box model contains only two reactions:



830 Where k and k' are rate constants of the reactions. The differences in rate constants were calculated
831 by assuming an $\alpha(\text{NO}_2\text{-NO})$ value of 1.0275. Six simulations were conducted at various initial NO
832 (with $\delta^{15}\text{N}=0\%$) and O₃ levels that were similar to our experiment. Then the $\delta^{15}\text{N}$ values of NO
833 and NO₂ during the simulation were calculated from the model and were shown in Figure B1,
834 suggesting that in our experimental condition, all systems should reach isotopic equilibrium within
835 1 hr.

836



837

838 Figure B1 Simulated NO-NO₂ isotopic equilibrium process in the chamber at various NO and O₃
 839 concentrations.

Formatted: Justified, Line spacing: Double

840 **Appendix C. Deriving Equations 7 and 8**

841 When the system (R1-R6) reaches steady-state, we have:

842
$$\frac{d[^{15}\text{NO}_2]/dt=0 \quad \text{Eq. (C1)}$$

843 Therefore, using R1-R6:

844
$$k_1 [^{15}\text{NO}_2][^{14}\text{NO}] + j(\text{NO}_2)\alpha_1 [^{15}\text{NO}_2] =$$

845
$$k_5\alpha_2 [^{15}\text{NO}][\text{O}_3] + k_1\alpha(\text{NO}_2-\text{NO}) [^{15}\text{NO}][^{14}\text{NO}_2] \quad \text{Eq. (C2)}$$

Formatted: Indent: Left: 0", First line: 0"

846 From here we refer $^{14}\text{NO}_2$ and ^{14}NO as NO_2 and NO for convenience, rearrange the above equation,
847 we get:

848
$$\frac{[^{15}\text{NO}_2]}{[^{15}\text{NO}]} = \frac{k_5\alpha_2[\text{O}_3] + k_1\alpha(\text{NO}_2-\text{NO}) [\text{NO}_2]}{j_{\text{NO}_2}\alpha_1 + k_1[\text{NO}]} \quad \text{Eq. (C3)}$$

849 Meantime, since the Leighton cycle reaction still holds for the majority isotopes (NO and NO_2),
850 we have:

851
$$j_{\text{NO}_2}[\text{NO}_2] = k_5[\text{NO}][\text{O}_3] \quad \text{Eq. (C4)}$$

852 Thus,

853
$$\frac{[\text{NO}_2]}{[\text{NO}]} = \frac{k_5 \times [\text{O}_3]}{j_{\text{NO}_2}} \quad \text{Eq. (C5)}$$

854 From the text, when $j_{\text{NO}_2} > 0$, we defined $A = \tau_{\text{exchange}}/\tau_{\text{photo}} = j_{\text{NO}_2}/(k_1 \times [\text{NO}])$. Using the above
855 equations, we know:

856
$$\frac{j_{\text{NO}_2}}{[\text{NO}]} = \frac{k_5[\text{O}_3]}{[\text{NO}_2]} = Ak_1 \quad \text{Eq. (C6)}$$

Formatted: Indent: Left: 2", First line: 0.5"

857
$$\frac{j_{\text{NO}_2}}{k_1[\text{NO}]} = \frac{k_5[\text{O}_3]}{k_1[\text{NO}_2]} = A \quad \text{Eq. (C7)}$$

858 Next, to calculate $\delta(\text{NO}_2) - \delta(\text{NO})$, we use the definition of delta notation:

859
$$\delta(\text{NO}_2) - \delta(\text{NO}) = R_{\text{NO}_2}/R_{\text{std}} - R_{\text{NO}}/R_{\text{std}} = (R_{\text{NO}_2}/R_{\text{NO}} - 1)(1 + \delta(\text{NO})) \quad \text{Eq. (C8)}$$

Formatted: Indent: Left: 0.5", First line: 0.5"

860

861
$$\frac{R_{NO_2}}{R_{NO}} = \frac{[^{15}NO_2][NO]}{[^{15}NO][NO_2]} = \frac{k_5\alpha_2[O_3][NO] + k_1\alpha(NO_2-NO)[NO_2][NO]}{j_{NO_2}\alpha_1[NO_2] + k_1[NO][NO_2]} \quad \text{Eq. (C9)}$$

Formatted: Indent: Left: 0.5", First line: 0.5"

862 Divide both side by $k_1[NO][NO_2]$:

863
$$\frac{R_{NO_2}}{R_{NO}} = \frac{\frac{k_5\alpha_2[O_3]}{k_1[NO_2]} + \alpha(NO_2-NO)}{\frac{j_{NO_2}\alpha_1}{k_1[NO]} + 1} \quad \text{Eq. (C10)}$$

Formatted: Indent: Left: 2", First line: 0.5"

864 Rearrange and substitute $\frac{k_5[O_3]}{k_1[NO_2]}$ and $\frac{j_{NO_2}}{k_1[NO]}$ with A:

865
$$\frac{R_{NO_2}}{R_{NO}} = \frac{\alpha_2 \times A + \alpha(NO_2-NO)}{\alpha_1 \times A + 1} \quad \text{Eq. (C11)}$$

Formatted: Indent: Left: 2", First line: 0.5"

866
$$\frac{R_{NO_2}}{R_{NO}} - 1 = \frac{(\alpha_2 - \alpha_1) \times A + \alpha(NO_2-NO) - 1}{\alpha_1 \times A + 1} \quad \text{Eq. (C12)}$$

Formatted: Indent: Left: 1.5", First line: 0.5"

867 Thus,

868
$$\delta(NO_2) - \delta(NO) = \frac{(\alpha_2 - \alpha_1) \times A + \alpha(NO_2-NO) - 1}{\alpha_1 \times A + 1} (1 + \delta(NO)) \quad \text{Eq. (C13)}$$

869 Since $\alpha_1 \approx 1$, $\alpha_1 \times A + 1 \approx 1 + A$ this equation can be further simplified to Eq. 7:

870
$$\delta(NO_2) - \delta(NO) = \frac{(\alpha_2 - \alpha_1) \times A + \alpha(NO_2-NO) - 1}{A + 1} (1 + \delta(NO)) \quad \text{Eq. (C14)}$$

Formatted: Indent: Left: 1", First line: 0.5"

871 Then, using mass balance:

872
$$\delta(NO_2) f(NO_2) + \delta(NO) (1 - f(NO_2)) = \delta(NO_x) \quad \text{Eq. (C15)}$$

Formatted: Indent: Left: 1.5"

Formatted: Subscript

873 We can derive Eq. 8:

874
$$\delta(NO_2) - \delta(NO_x) = \frac{(\alpha_2 - \alpha_1) \times A + \alpha(NO_2-NO) - 1}{A + 1} (1 + \delta(NO)) (1 - f(NO_2)) \quad \text{Eq. (C16)}$$

Formatted: Indent: Left: 1", Line spacing: Double

Formatted: Font: Not Italic